Published in final edited form as:
Environ Sci Technol. 2012 July 17; 46(14): 7717–7724. doi:10.1021/es301377y.

Graphene-Based Environmental Barriers

Fei Guo, **Gregory Silverberg**, **Shin Bowers**, **Sang-Pil Kim**, **Dibakar Datta**, **Vivek Shenoy**, and **Robert H. Hurt***
School of Engineering, Institute for Molecular and Nanoscale Innovation, Brown University, Providence, Rhode Island

Abstract

Many environmental technologies rely on containment by engineered barriers that inhibit the release or transport of toxicants. Graphene is a new, atomically thin, two-dimensional sheet material, whose aspect ratio, chemical resistance, flexibility, and impermeability make it a promising candidate for inclusion in a next generation of engineered barriers. Here we show that ultrathin graphene oxide (GO) films can serve as effective barriers for both liquid and vapor permeants. First, GO deposition on porous substrates is shown to block convective flow at much lower mass loadings than other carbon nanomaterials, and can achieve hydraulic conductivities of 5×10^{-12} cm/s or lower. Second we show that ultrathin GO films of only 20 nm thickness coated on polyethylene films reduce their vapor permeability by 90% using elemental mercury as a model vapor toxicant. The barrier performance of GO in this thin-film configuration is much better than the Nielsen model limit, which describes ideal behavior of flake-like fillers uniformly imbedded in a polymer. The Hg barrier performance of GO films is found to be sensitive to residual water in the films, which is consistent with molecular dynamics (MD) simulations that show lateral diffusion of Hg atoms in graphene interlayer spaces that have been expanded by hydration.

INTRODUCTION

Approaches for managing toxic substances include capture and removal, destruction, chemical transformation to low-toxicity products, and source containment. In many practical scenarios, containment is the technology of choice due to cost and simplicity. The containment approach typically relies on engineered barriers that prevent or inhibit toxicant transport to the open environment or to compartments where exposures are more likely for humans or sensitive environmental receptors.

The containment approach encompasses a wide range of technologies that include personal protective equipment for workers or military personnel, geomembranes for landfill liners and caps,[1] sealants for surfaces containing lead paint, architectural vapor barriers to protect buildings from the intrusion of radon or volatile organic compounds, vertical subsurface barriers that are either passive[2] or reactive,[3] in situ sediment caps[4] sealants or coatings to suppress indoor formaldehyde release from manufactured wood products, or tarps as transport barriers for soil fumigants.[5] Suppressing the transport or release of toxicants is also important in shipping and recycling of wastes containing volatile mercury[6, 7] which permeates through most bag and box materials, and in food and pharmaceutical packaging,

*corresponding author: Robert Hurt, School of Engineering, Brown University, Providence, RI 02012, Tel: 401 863-2685, Fax: 401 863-9120, Robert_Hurt@brown.edu.

Supporting information
Graphene oxide synthesis and characterization, experimental setup for hydraulic sealing measurement, raw data of mercury vapor concentration, modeling and molecular dynamics simulations. This material is available free of charge via the Internet at http://pubs.acs.org.

where inks, monomers, and plasticizers can leach through or from the polymer packaging into the product. Improved barrier fillers or inner linings may be able to reduce the amount of “leachables and extractables” that find their way into foods and drugs.

Many synthetic barriers are based on polymers, and most commodity polymers are not effective barriers to small molecule permeation, especially in the vapor phase. There is strong motivation to identify low-cost methods for improving the barrier performance of polymers.[8] A new approach for designing transport barriers makes use of graphene, single-atom-thick sheet of carbon observed in 1961[59] and first isolated from crystalline graphite in 2004.[9] The perfect graphene monolayer is impermeable even to He atoms,[10, 11] and its atomically thin structure could allow it to perform its barrier function at very low mass loadings and thus low cost and weight. The economical forms of graphene available now, however, have limited lateral dimension on the scale of microns, and the technical challenge is to assemble these building blocks into practical materials or composites that meet the requirements for specific barrier applications.

The work to date on graphene-based barriers has focused on gases (oxygen, helium, hydrogen, nitrogen, water vapor)[12–15,61,62] with a limited amount of work on organic solvents (ethanol, hexane).[15] In the environmental literature, graphene materials have been explored as sorbents,[16, 17] sensors,[18] photocatalysts,[19] or electrodes for capacitive deionization[20] but there has been no work to our knowledge on graphene-based barriers to toxicant transport, i.e. barriers for environmental containment technologies.

Here we report on the first exploration of graphene materials as environmental barriers to toxicant transport. We focus on graphene oxide building blocks, which can be processed in water, and perform proof-of-principle experiments on both vapor barriers and hydraulic (liquid) barriers. For the vapor demonstration, elemental mercury was adopted as a model vapor toxicant that is known to permeate commodity polymer films.[6, 7] We show that ultrathin GO films with as few as 25 layers (thickness ~ 20 nm) can reduce Hg permeation by 90%, and that the multilayer film geometry far outperforms the imbedded sheet geometry (common “Nielsen” configuration) due to suppression of horizontal migration between the layers. The barrier mechanism for these ultrathin GO films is investigated by studying moisture dependence and through analytical modeling and molecular dynamics simulations of Hg atom diffusion in confined inter-laminar spaces.

MATERIALS AND METHODS

Materials

Graphene oxide was prepared using a modified Hummer’s method,[21] and characterized by atomic force microscopy (AFM), scanning electron microscopy (SEM), and dynamic light scattering (DLS) (Supporting info). In aqueous suspension it exists primarily as monolayer sheets from 0.3–3 μm (volume mean diameter: ~ 1.7 μm) (Fig. S2) in lateral dimension. A set of commercial polymer film materials was purchased from McMaster-Carr and cut into 15 cm diameter disks for permeability testing. The work on graphene hydraulic sealants used 1D and 3D reference materials: multiwalled carbon nanotubes from Mitsui (nominal diameter 20–100 nm and length ~15 μm) and carbon black (Printex 90, primary particle diameter 14 nm).

Hydraulic Sealing Experiments

Suspensions of graphene oxide, carbon nanotubes, and carbon black were subjected to pressure-driven flow through syringe filters (Anotop 25: Whatman Ltd., pore size 20 nm, filtration area 4.78 cm^2; or Nylon syringe filters: Cameo 17GN, pore size 220 nm, filtration area 1.0 cm^2) using a syringe pump (Sage 361) at 1 mL/min (Fig. S4). The hydraulic

pressure drop was monitored over time by an upstream pressure sensor (USB output PX409, Omega).

Graphene Film Fabrication

Based on significant preliminary testing, drop casting on cationic surfactant-treated polymer surfaces was determined to be a suitable method for generating uniform graphene oxide films. Other techniques such as spin-coating have been reported,[63,64] but the drop casting technique allows direct calculation of the coating mass and estimation of mean layer number. Polyethylene was chosen as the base polymer substrate. A circular polyethylene sheet with a diameter of 20 cm was cleaned with ethanol and nanopure water, and immersed in a shallow pool of 173 ppm cetyl trimethylammonium bromide (CTAB) for 10 minutes to increase surface hydrophilicity and impart positive charge. The sheet was dried at 70°C for 60 minutes and stretched over a 20 cm glass plate and secured with adhesive tape to eliminate wrinkles and creases. The GO suspension was diluted (typically 0.05 – 0.5 mg/mL), and 25mL of the dilution was drop cast in the center of the polyethylene sheet. The sample, consisting of glass plate, polyethylene sheet, CTAB layer, and GO drop, was dried in air or placed in the drying oven at 70°C for 48 hours. The layered film was then removed from the glass plate and its mercury vapor permeability was tested.

Film Permeability Testing

Measurements of vapor permeability require special equipment to eliminate mass transfer resistances in the gas spaces on either side of the test film. We were unable to find commercial equipment for mercury vapor, so a custom device (Fig. 1) was designed and tested. This glass mercury diffusion cell uses Viton O-rings to seal a polymer film or polymer/GO film over a standing pool of elemental mercury of 50 mm depth 74 mm diameter (Fig. 1). To reduce gas-phase transport resistance, the membrane was positioned only 2 mm above the pool surface giving a mass transfer coefficient of order D/δ (stagnant gas limit), which represents less than 5% of the resistance of the polymer film. Downstream of the membrane, a miniature electric fan forces convective flow onto the test surface which reduces gas-phase transport resistance to small values. The mercury concentration in the exit stream (200 cc/min) was determined by a semi-continuous gold-trap atomic fluorescence mercury vapor analyzer (Sir Galahad, PSAnalytical) and the mercury molar flow converted to permeation flux. The analysis stream induced an equivalent in-flow of room air (200 cc/min) from a side pore in the upper half of the cell, which also serves as a feed for the electrical wiring. To avoid mercury contamination above the film, the cap was kept separate from the pool between tests and was purged with compressed air for several minutes between each test. A thick impermeable control film of polyethylene terephthalate was inserted between each test until baseline concentrations of exit Hg reached suitably low baseline values.

Molecular Dynamics Simulations

MD methods were used to study the diffusion of Hg atoms through the interlayer spaces of GO multilayer films as a function of water content. Medhekar *et al.* showed that the interlayer spacing of GO can be controlled by the H_2O fraction which determines the extent and collective strength of interlayer hydrogen bond networks.[49] We combined sets of MD potentials for Hg, H_2O, and C by adopting the potential hybrid method which enables the use of multiple potentials in one simulation.[57] For describing water interactions, SPC/E water model is employed[56] and the long-range Coulombic interactions are computed in conjunction with the particle-particle particle-mesh solver.[60] Other interactions such as Hg-Hg and C-C are assumed to be Van der Waals interactions described by the Lennard-Jones 12–6 potential.[55] The use of the simple LJ potential for describing the C-C interactions is sufficient because all graphene sheets are assumed to be static. The standard Lorentz-

Berthelot mixing rules are utilized for obtaining LJ potential parameters for the cross-interactions. The cutoff distance for all interactions is set to 10 Å. Periodic boundary conditions are imposed laterally to eliminate edge effects. The initial spacing between the sheets is set at 20Å and the gap is closed at constant velocity until the desired interlayer distance is reached.

RESULTS

Graphene oxide as a hydraulic sealant

In early, unrelated experiments we found it difficult to remove graphene oxide from suspension by centrifugal ultrafiltration. This technique has been observed to work for the separation of a variety of other nanomaterials, including those as small as 2–5 nm,[22] but for GO a portion of the solution appeared unable to pass the ultrafilter. We hypothesized that GO was unusually effective at blocking convective liquid flows through porous substrates and carried out systematic experiments to test this hypothesis. Aqueous suspensions of GO (2D material) along with a 3D reference material (aryl-sulfonated carbon black particles), and a 2D reference material (aryl-sulfonated carbon nanotubes) with the same mass concentration were uniformly pumped through a syringe filter and the pressure drop monitored over time. Only graphene oxide produces a diverging pressure drop after several ml of flow (Fig. 2A). GO forms a dense surface film with a micron-scale tiling or wrinkle pattern (Fig. 2B), while the 3D and 1D material form porous deposits. The development of the sealant film can be tracked at higher resolution by a set of time-resolved experiments using different GO concentrations (Fig. 2C). Figure D collapses that data set by renormalization using GO mass on X-axis calculated as $V_{\text{filtrate}} \times C_{\text{GO}}$, which represents the total GO mass collected at time t. The total amount of GO deposited appears to determine the sealant performance. Beyond 40 μg deposited or about 160 GO layers, the porous material is effectively sealed irrespective of the applied pressure. At a typical wet GO spacing of about 1 nm, the 50-layer stack in Fig. 2A represents a film of only 50 nm in thickness. Barrier materials to convective water flow are often characterized by the hydraulic conductivity, K, defined by $v = K\Delta P/\delta_{\text{film}}$. At 50 nm, $K = 5\times10^{-13}$ m^2/bar-sec, or with pressure expressed in equivalent water column height, $K = 5\times10^{-12}$ cm/s. At the end of our experiment, ΔP is increasing rapidly, which suggests that K values will continue to decrease rapidly as deposition continues beyond the range accessible to our experiment (Fig. 2).

Few-layer graphene oxide vapor barriers

Elemental mercury has been reported to pass readily through common polymers used in fluorescent lamp disposal and recycling,[6, 7] and was chosen as a model permeating vapor toxicant for this study. Prior to characterizing the barrier enhancement properties of GO films, we needed quantitative data on Hg permeability in the base polymers, and we could not find systematic data in the literature. We therefore adopted, as a secondary goal for this study, to measure Hg-vapor permeability constants for a range of commercial polymers, which could help guide the selection of containment materials for Hg-containing products and wastes.

Measurements of Hg vapor permeability in polymer films—We applied the custom diffusion cell in Fig. 1 to a range of commercial polymers in sheet form (Figure 3). For sheets, the permeation rate R (mol/s) is given by: $R = AP\Delta C$, where A is the membrane area and P is the permeability, $P = DH/\delta$, where D is the diffusion coefficient of Hg in the polymer, δ the film thickness, and H the partition coefficient of Hg in the two phases at equilibrium ($C^{\text{polymer}}/C^{\text{vapor}}$). In these experiments the pre-membrane concentration is saturated Hg vapor (18,000 μg/m^3 at 23°C),[23] and the post-membrane concentration is

approximately equal to the measured steady state exit concentration due to active stirring in the head space. Example raw data is shown in Fig. S5. For highly permeable materials, membranes were stacked to increase resistance and in all cases we report the permeability coefficient (*DH*), which unlike the permeability itself (*DH*/δ) is a material property independent of sheet thickness. Figure 3 shows that common polymers exhibit a wide range of permeability coefficients for vapor-phase Hg (atomic diameter: 0.3 nm) and that the values are of the same order of magnitude as values for small gases O_2 (0.35 nm), N_2 (0.37 nm) or CO_2 (0.4 nm).[24] Nylon, acetate, and polyester show the lowest permeability coefficients, followed by high-density polyethylene at ~ 5× higher permeability, and the elastomers (neoprene, silicone).

Graphene oxide for enhanced barrier performance—Low-density polyethylene (LDPE) films of 50 μm thickness were chosen as a model substrate for graphene-based barrier enhancement. The conventional approach to barrier enhancement is to add the low-permeability component as filler uniformly distributed in the polymer matrix. Mineral flakes are a common filler,[26–30] and they suppress permeation better than spheres or cylinders at equal volume percentage.[31] The primary mechanism of barrier enhancement is an increase the diffusive path length (Fig. 4) described by Eq. (1), the simple Nielsen model.[32]

$$\frac{P}{P_m}=\frac{1-\varphi}{1+0.5\alpha\varphi} \quad (1)$$

Here P is the permeability of the composite; P_m is the permeability of the matrix material; is φ the volume fraction of the flake fillers; α is the aspect ratio (lateral size/thickness). The performance of fillers in the imbedded (Nielsen) configuration is limited because it does not necessarily alter the diffusion coefficient in the polymer phase, but only increases path length.

Our concept here was to strive for greater barrier enhancement by collapsing the GO flakes into a film that also restricts horizontal migration (see Fig. 4). Of several ways to make GO films,[12–14, 33–42] we chose to directly cast GO suspension onto polymer membranes pretreated with the cationic surfactant CTAB to impart hydrophilicity and positive charge. The thickness of the films can be varied by GO concentration and liquid volume. The GO laminates are observed to be adherent and mechanically stable on the polyethylene surfaces even after hand folding. The polymers with GO nanofilms are noticably darker than the untreated polymers but still transparent (Fig. 4).

Figure 4 shows that the film configuration is indeed highly effective as a barrier enhancement. GO films of only 10 nm thickness can suppress Hg-vapor permeability by 60%, and 20 nm coatings can achieve ~ 90% reduction. The barrier suppression is much greater than that expected for ideal imbedding, as predicted by the Nielsen model (Eq.1) for horizontally aligned single-sheet flakes at the same GO/polymer mass loading (reference curve in Fig. 4). Many experimental studies with imbedded clay or graphene materials do not achieve the Nielsen limit due to non-uniform mixing or to misalignment, so the ability of these films to exceed the Nielsen limit is significant.

The film results can also be compared to a simple model in which thin disks randomly deposit on the polymer surface and cast diffusion shadows that inhibit transport into and through the film. In the limit of thin polymer films, this blockage is directly proportional to the fractional coverage, if the disks fall by an independent Poisson process that allows overlap.[43] In this case the inhibition is:

$$\frac{P}{P_m} \approx Q = e^{-\lambda A} = e^{-n} \quad (2)$$

where P/P_m is the relative permeability, Q the proportion of uncovered area which equals to the relative permeability; λ the density of disk centers in counts per square areal unit; A is the disk area; n is the number of layers (see Fig. 4 curve).

The permeability of GO-coated polyester was found to be sensitive to drying conditions. Figure 5 shows that films dried at room temperature show significantly higher Hg-vapor permeabilities than films dried at 70 °C. We suspected that this effect was due to lateral diffusion of Hg through the expanded layer structure associated with interlayer water.[15] We therefore applied X-ray diffraction to the films and found that high-temperature drying decreased interlayer spacing consistent with interstitial water removal (Fig. 5). Nair et al. have recently reported that drying improves the barrier properties of GO films to small gas molecules[15] and the XRD results were used along with MD simulations to gain insight into the molecular events associated with Hg permeation (see Discussion).

DISCUSSION AND MODELLING

This data set shows that casting graphene oxide from aqueous suspension onto polymer or porous ceramic substrates can produce adherent, ultrathin films with very good hydraulic and mercury vapor barrier properties. The hydraulic barrier performance is believed to be due to the sealing effect of GO sheets that deposit with their axes parallel to substrates containing submicron pores. The hydraulic conductivities are much lower for GO than 1D and 3D carbon-based nanomaterials. Although monolayer graphene is in principle an effective barrier, here the finite lateral size of the GO sheets (~ 1μm) requires that covering films be built up gradually by deposition, good hydraulic barrier performance is achieved here only after statistical tiling or overlapping of at least 25–50 layers. At 50 layers we calculate a hydraulic conductivity of 5×10^{-12} cm/s, which is lower than natural geological materials classified as “impervious” such as limestone, granite, or unweathered clay. Extrapolation of the curves in Fig. 2 suggest that lower values are likely achievable by further deposition.

As vapor barriers, ultrathin GO coatings on polymers are also effective for the model vapor toxicant, mercury. The Hg permeability of polyethylene can be reduced by 90% with as few as 25 GO layers (~ 20 nm films) that represent a very low mass fraction of the base polymer (0.05 wt-% for 20 nm films on 50 μm polyethylene), which is promising for practical applications. Especially noteworthy is the ability of the films to achieve barrier properties that exceed the well-known Nielsen limit for ideal imbedding of flake-like fillers oriented parallel to the substrate (Fig. 4 sketch and reference curve). The barrier performace seen in the present work can be compared to that of Kim et al.,[14] which uses imbedded graphene oxide to decrease the permeability of PVA to oxygen. Adding 0.3 wt-% GO to PVA decreased the permeability of their layered structure by P/P_o = 0.257/1.27 or a reduction of 80%. The film configuration in the present work achieves 90% reduction with 1/6 of that mass loading. Note that Kim et al. report improved performance if the GO is reduced with hydrazine (P/P_o = 0.0514/1.27 or 95% reduction at 0.3 wt-%). Using nano-clay in PVA, Yuen et al.[44] report P/P_o of 29% at 5 wt.% clay loading. Compton et al. report P/P_o of 50% at about 1 wt-% graphene addition to polystyrene films.[12] In comparison to these benchmarks, the ultrathin graphene oxide films prepared here achieve much improved barrier performance at equivalent mass loadings. Of course the imbedded configuration offers the practical advantage that the graphene filler is mechanically stabilized within the polymer sheet.

For further development of this technology it would be useful to understand the mechanisms that limit barrier performance. The small amount of residual Hg vapor "leakage" through GO films seen here may be due to (i) atomic defects in the GO sheets,[45, 46] (ii) imperfect depositional assembly that lead to microscopic flaws in the covering film, or (iii) solute permeation through the multilayer stacks involving lateral diffusion through interlayer spaces to find pathways around individual GO sheets (Fig. S6). The observation that permeability is sensitive to drying conditions provides insight into mechanism (iii).

GO is well known to hold water molecules in H-bonded configuration with its oxygen-containing functional groups,[47–49] and the bound water can increase interlayer spacing.[33, 49–51] The O-containing groups on GO tend to cluster leaving unfunctionalized graphene patches that can participate in π-bonding and adsorption of hydrophobic molecules.[37, 52, 53] Nair et al.[15] have recently reported that water vapor can facilitate the permeation of gases through GO multilayer films. They propose that water molecules associated with oxygen-containing functional groups act as pillars to increase the interlayer spacing, and the unfunctionalized patches lying between these H-bonded pillars form percolating channels that allow molecular transport through and across the films. Removing water reduces interlayer spacing and effectively stops the permeation of small gases.[15] We hypothesized that residual water from incomplete drying is acting in the same way in our Fig. 5 data.

To test this hypothesis we applied the Nielsen model to a hydrated GO multilayer, where the water phase now becomes the matrix through which the permeating species (here Hg) diffuses. The Nielsen model is derived for the dilute regime,[26, 54] so we modified it by accounting for excluded volume in the regime where the filler (GO) is more concentrated. Eq.(3) shows a modified Nielsen model in which we subtract the excluded volume associated with the finite size of the permeating molecule, σ.

$$P = DH\frac{d_{GO} - W - \sigma}{n d_{GO}\left(d_{GO} + \frac{1}{2}\alpha W\right)} \quad (3)$$

Here H is the partition coefficient (obtained from Hg solubility in water); D is the effective diffusivity of Hg in the interlayer space; W is the thickness of an unfunctionalized graphene sheet including its electron clouds (0.34 nm); α is the aspect ratio of the plate fillers (lateral size/thickness); n is the number of layers in the GO film, and d_{GO} is the interlayer distance (distance between nuclear planes) of GO, which can be measured by XRD. We use the unfunctionalized sheet thickness to model the unfunctionalized regions in GO, which are expected to be the primary diffusion paths. The primary unknown in this model is the effective diffusivity of Hg in the interlayer spaces.

To understand Hg diffusion in hydrated GO interlayer spaces and to estimate D, we carried out MD simulations involving a single Hg atom between two graphene sheets of 6.3 nm lateral dimension containing interlayer water (Fig. 6). Details of the methods and potential functions have been described previously[55] and in the supporting information. At the chosen layer spacing, water molecules are introduced into the available space at their liquid phase density (33.3 molecules per nm^3) and the temperature of the system except carbon atoms is kept at 300K controlled by a Berendsen thermostat, which rescales their velocities every timestep (each MD time step Δt=1.0 fs).[56] The mean-squared displacement (MSD) is used to calculate the mercury diffusion coefficient D_0 by:

$$D_0 = \frac{1}{6t} \left\langle |\boldsymbol{r}_i(t) - \boldsymbol{r}_i(0)|^2 \right\rangle \quad (4)$$

applied after the system is fully relaxed. The Hg D_0 is obtained from the asymptotic slope of the MSD for 500 ps of MD simulations. All simulations are carried out by the LAMMPS package.[57]

Figure 6 shows Hg diffusion coefficients as a function of interlayer spacing. The Hg atom is immobile at spacings less than 7 Å and becomes increasingly mobile above 8 Å. All relevant values are well below the diffusivity of Hg in bulk water (1.88×10^{-5} cm^2/sec at 300 K [58]). We observe that Hg mobility is related to the mobility of the surrounding water molecules. Below 7 Å the simulations show that water forms an immobile monolayer that traps the Hg, while increasing spacing leads to a water double layer that enables Hg atom to move by positional replacement. These results provide insight into interlayer Hg diffusion and can be used to complete the model in Eq. (3).

Figure 7 shows the results of the Nielson model modified for excluded volume and using the interlayer diffusivity values from the MD simulations of Fig. 6. The predicted permeabilities show the same trend as the data in Fig. 5 as a function of interlayer spacing, which supports mechanism (iii) above as the cause of the moisture dependence. Lateral diffusion of Hg through hydrated and expanded interlayer spaces is consistent with the observed trends.

In conclusion, graphene-based materials show great promise for a next generation of environmental barrier materials. These atomically thin materials provide low hydraulic conductivity and low Hg-vapor permeability at very low areal density, which is promising for practical, cost effective materials. Nair et al.[15] report essentially no vapor permeability in the dry state, but their films are much thicker (0.1 – 1 μm) and thus their results may be seen as consistent with the present ones for ultrathin 25 nm films. The excellent barrier performance exhibited for liquid water and mercury vapor are not believed to be highly chemically specific properties, and could likely be extended to a wide range of toxicants. The observed moisture sensitivity suggests one could create tunable or selective barriers by altering residual water through humidity control. Much more work is needed on the large-scale fabrication, permeability, and mechanical stability of graphene-based environmental barriers.

Supplementary Material

Refer to Web version on PubMed Central for supplementary material.

Acknowledgments

Financial support for this work was provided by the NIEHS Superfund Research Program grant P42 ES013660, and the US National Science Foundation grant CBET-1132446. The technical contributions of Megan Creighton, Paul Waltz, and Indrek Kulaots at Brown are gratefully acknowledged.

References

1. Rowe, RK. Barrier systems for waste disposal facilities. 2. Spon Press; New York: 2004.
2. Filz GM, Widdowson MA, Little JC. Barrier-controlled monitored natural attenuation. Environ Sci Technol. 2001; 35(15):3225–3230. [PubMed: 11506009]
3. Shimotori T, Nuxoll EE, Cussler EL, Arnold WA. A polymer membrane containing Fe-0 as a contaminant barrier. Environ Sci Technol. 2004; 38(7):2264–2270. [PubMed: 15112833]

4. McDonough KM, Murphy P, Olsta J, Zhu Y, Reible D, Lowry GV. Development and Placement of a Sorbent-Amended Thin Layer Sediment Cap in the Anacostia River. Soil and Sediment Contamination: An International Journal. 2007; 16(3):313–322.
5. Wang D, Yates SR, Ernst FF, Gan J, Jury WA. Reducing methyl bromide emission with a high barrier plastic film and reduced dosage. Environ Sci Technol. 1997; 31(12):3686–3691.
6. Johnson NC, Manchester S, Sarin L, Gao YM, Kulaots I, Hurt RH. Mercury vapor release from broken compact fluorescent lamps and in situ capture by new nanomaterial sorbents. Environ Sci Technol. 2008; 42(15):5772–5778. [PubMed: 18754507]
7. Lee B, Sarin L, Johnson NC, Hurt RH. A Nano-Selenium Reactive Barrier Approach for Managing Mercury over the Life-Cycle of Compact Fluorescent Lamps. Environ Sci Technol. 2009; 43(15): 5915–5920. [PubMed: 19731697]
8. Sekelik DJ, Stepanov EV, Nazarenko S, Schiraldi D, Hiltner A, Baer E. Oxygen barrier properties of crystallized and talc-filled poly(ethylene terephthalate). J Polym Sci Pol Phys. 1999; 37(8):847–857.
9. Novoselov KS, Geim AK, Morozov SV, Jiang D, Zhang Y, Dubonos SV, Grigorieva IV, Firsov AA. Electric field effect in atomically thin carbon films. Science. 2004; 306(5696):666–669. [PubMed: 15499015]
10. Bunch JS, Verbridge SS, Alden JS, van der Zande AM, Parpia JM, Craighead HG, McEuen PL. Impermeable atomic membranes from graphene sheets. Nano Lett. 2008; 8(8):2458–2462. [PubMed: 18630972]
11. Leenaerts O, Partoens B, Peeters FM, Graphene. A perfect nanoballoon. Appl Phys Lett. 2008; 93(19)
12. Compton OC, Kim S, Pierre C, Torkelson JM, Nguyen ST. Crumpled Graphene Nanosheets as Highly Effective Barrier Property Enhancers. Adv Mater. 2010; 22(42):4759. [PubMed: 20830709]
13. Kim H, Miura Y, Macosko CW. Graphene/Polyurethane Nanocomposites for Improved Gas Barrier and Electrical Conductivity. Chem Mater. 2010; 22(11):3441–3450.
14. Kim HM, Lee JK, Lee HS. Transparent and high gas barrier films based on poly(vinyl alcohol)/ graphene oxide composites. Thin Solid Films. 2011; 519(22):7766–7771.
15. Nair RR, Wu HA, Jayaram PN, Grigorieva IV, Geim AK. Unimpeded Permeation of Water Through Helium-Leak-Tight Graphene-Based Membranes. Science. 2012; 335(6067):442–444. [PubMed: 22282806]
16. Zhao GX, Li JX, Ren XM, Chen CL, Wang XK. Few-Layered Graphene Oxide Nanosheets As Superior Sorbents for Heavy Metal Ion Pollution Management. Environ Sci Technol. 2011; 45(24):10454–10462. [PubMed: 22070750]
17. Zhu JH, Wei SY, Gu HB, Rapole SB, Wang Q, Luo ZP, Haldolaarachchige N, Young DP, Guo ZH. One-Pot Synthesis of Magnetic Graphene Nanocomposites Decorated with Core@Double-shell Nanoparticles for Fast Chromium Removal. Environ Sci Technol. 2012; 46(2):977–985. [PubMed: 22126606]
18. Ratinac KR, Yang WR, Ringer SP, Braet F. Toward Ubiquitous Environmental Gas Sensors-Capitalizing on the Promise of Graphene. Environ Sci Technol. 2010; 44(4):1167–1176. [PubMed: 20099803]
19. Zhang H, Fan XF, Quan X, Chen S, Yu HT. Graphene Sheets Grafted Ag@AgCl Hybrid with Enhanced Plasmonic Photocatalytic Activity under Visible Light. Environ Sci Technol. 2011; 45(13):5731–5736. [PubMed: 21663048]
20. Li HB, Zou LD, Pan LK, Sun Z. Novel Graphene-Like Electrodes for Capacitive Deionization. Environ Sci Technol. 2010; 44(22):8692–8697. [PubMed: 20964326]
21. Kim F, Luo JY, Cruz-Silva R, Cote LJ, Sohn K, Huang JX. Self-Propagating Domino-like Reactions in Oxidized Graphite. Adv Funct Mater. 2010; 20(17):2867–2873.
22. Liu JY, Hurt RH. Ion Release Kinetics and Particle Persistence in Aqueous Nano-Silver Colloids. Environ Sci Technol. 2010; 44(6):2169–2175. [PubMed: 20175529]
23. Huber ML, Laesecke A, Friend DG. Correlation for the vapor pressure of mercury. Ind Eng Chem Res. 2006; 45(21):7351–7361.

24. Hirschfelder, JO.; Bird, RB.; Curtiss, CF. Molecular theory of gases and liquids. Wiley; New York: 1954.
25. Plastics Design Library. Permeability and other film properties of plastics and elastomers. Plastics Design Library; Norwich, NY: 1995.
26. Cussler EL, Hughes SE, Ward WJ, Aris R. Barrier Membranes. J Membrane Sci. 1988; 38(2):161–174.
27. Eitzman DM, Melkote RR, Cussler EL. Barrier membranes with tipped impermeable flakes. Aiche J. 1996; 42(1):2–9.
28. Moggridge GD, Lape NK, Yang CF, Cussler EL. Barrier films using flakes and reactive additives. Prog Org Coat. 2003; 46(4):231–240.
29. Lape NK, Nuxoll EE, Cussler EL. Polydisperse flakes in barrier films. J Membrane Sci. 2004; 236(1):29–37.
30. Yang CF, Smyrl WH, Cussler EL. Flake alignment in composite coatings. J Membrane Sci. 2004; 231(1–2):1–12.
31. DeRocher JP, Gettelfinger BT, Wang JS, Nuxoll EE, Cussler EL. Barrier membranes with different sizes of aligned flakes. J Membrane Sci. 2005; 254(1–2):21–30.
32. Nielsen LE. Models for the Permeability of Filled Polymer Systems. Journal of Macromolecular Science: Part A - Chemistry. 1967; 1(5):929–942.
33. Stankovich S, Dikin DA, Piner RD, Kohlhaas KA, Kleinhammes A, Jia Y, Wu Y, Nguyen ST, Ruoff RS. Synthesis of graphene-based nanosheets via chemical reduction of exfoliated graphite oxide. Carbon. 2007; 45(7):1558–1565.
34. Eda G, Fanchini G, Chhowalla M. Large-area ultrathin films of reduced graphene oxide as a transparent and flexible electronic material. Nat Nanotechnol. 2008; 3(5):270–274. [PubMed: 18654522]
35. Eda G, Chhowalla M. Chemically Derived Graphene Oxide: Towards Large-Area Thin-Film Electronics Optoelectronics. Adv Mater. 2010; 22(22):2392–2415. [PubMed: 20432408]
36. Chen CM, Yang QH, Yang YG, Lv W, Wen YF, Hou PX, Wang MZ, Cheng HM. Self-Assembled Free-Standing Graphite Oxide Membrane. Adv Mater. 2009; 21(29):3007.
37. Guo F, Kim F, Han TH, Shenoy VB, Huang JX, Hurt RH. Hydration-Responsive Folding and Unfolding in Graphene Oxide Liquid Crystal Phases. ACS Nano. 2011; 5(10):8019–8025. [PubMed: 21877716]
38. Stankovich S, Dikin DA, Dommett GHB, Kohlhaas KM, Zimney EJ, Stach EA, Piner RD, Nguyen ST, Ruoff RS. Graphene-based composite materials. Nature. 2006; 442(7100):282–286. [PubMed: 16855586]
39. Li D, Muller MB, Gilje S, Kaner RB, Wallace GG. Processable aqueous dispersions of graphene nanosheets. Nat Nanotechnol. 2008; 3(2):101–105. [PubMed: 18654470]
40. Yamaguchi H, Eda G, Mattevi C, Kim H, Chhowalla M. Highly Uniform 300 mm Wafer-Scale Deposition of Single and Multilayered Chemically Derived Graphene Thin Films. ACS Nano. 2010; 4(1):524–528. [PubMed: 20050640]
41. Dikin DA, Stankovich S, Zimney EJ, Piner RD, Dommett GHB, Evmenenko G, Nguyen ST, Ruoff RS. Preparation and characterization of graphene oxide paper. Nature. 2007; 448(7152):457–460. [PubMed: 17653188]
42. Lee SH, Kim HW, Hwang JO, Lee WJ, Kwon J, Bielawski CW, Ruoff RS, Kim SO. Three-Dimensional Self-Assembly of Graphene Oxide Platelets into Mechanically Flexible Macroporous Carbon Films. Angew Chem Int Edit. 2010; 49(52):10084–10088.
43. Jupp DLB, Strahler AH, Woodcock CE. Autocorrelation and regularization in digital images. II. Simple image models. Geoscience and Remote Sensing, IEEE Transactions on. 1989; 27(3):247–258.
44. Yeun JH, Bang GS, Park BJ, Ham SK, Chang JH. Poly(vinyl alcohol) nanocomposite films: Thermooptical properties, morphology, and gas permeability. J Appl Polym Sci. 2006; 101(1): 591–596.
45. Gomez-Navarro C, Meyer JC, Sundaram RS, Chuvilin A, Kurasch S, Burghard M, Kern K, Kaiser U. Atomic Structure of Reduced Graphene Oxide. Nano Lett. 2010; 10(4):1144–1148. [PubMed: 20199057]

46. Bagri A, Mattevi C, Acik M, Chabal YJ, Chhowalla M, Shenoy VB. Structural evolution during the reduction of chemically derived graphene oxide. Nat Chem. 2010; 2(7):581–587. [PubMed: 20571578]
47. Szabo T, Berkesi O, Dekany I. DRIFT study of deuterium-exchanged graphite oxide. Carbon. 2005; 43(15):3186–3189.
48. Szabo T, Berkesi O, Forgo P, Josepovits K, Sanakis Y, Petridis D, Dekany I. Evolution of surface functional groups in a series of progressively oxidized graphite oxides. Chem Mater. 2006; 18(11): 2740–2749.
49. Medhekar NV, Ramasubramaniam A, Ruoff RS, Shenoy VB. Hydrogen Bond Networks in Graphene Oxide Composite Paper: Structure and Mechanical Properties. ACS Nano. 2010; 4(4): 2300–2306. [PubMed: 20380417]
50. Lerf A, Buchsteiner A, Pieper J, Schottl S, Dekany I, Szabo T, Boehm HP. Hydration behavior and dynamics of water molecules in graphite oxide. J Phys Chem Solids. 2006; 67(5–6):1106–1110.
51. Jeong HK, Lee YP, Jin MH, Kim ES, Bae JJ, Lee YH. Thermal stability of graphite oxide. Chem Phys Lett. 2009; 470(4–6):255–258.
52. Sanchez VC, Jachak A, Hurt RH, Kane AB. Biological Interactions of Graphene-Family Nanomaterials: An Interdisciplinary Review. Chemical Research in Toxicology. 2012; 25(1):15–34. [PubMed: 21954945]
53. Kim F, Cote LJ, Huang JX. Graphene Oxide: Surface Activity and Two-Dimensional Assembly. Adv Mater. 2010; 22(17):1954–1958. [PubMed: 20432227]
54. Lu CS, Mai YW. Permeability modelling of polymer-layered silicate nanocomposites. Compos Sci Technol. 2007; 67(14):2895–2902.
55. Chen JY, Kutana A, Collier CP, Giapis KP. Electrowetting in carbon nanotubes. Science. 2005; 310(5753):1480–1483. [PubMed: 16322454]
56. Berendsen HJC, Postma JPM, Vangunsteren WF, Dinola A, Haak JR. Molecular-Dynamics with Coupling to an External Bath. J Chem Phys. 1984; 81(8):3684–3690.
57. Plimpton S. Fast Parallel Algorithms for Short-Range Molecular-Dynamics. J Comput Phys. 1995; 117(1):1–19.
58. Kuss J, Holzmann J, Ludwig R. An Elemental Mercury Diffusion Coefficient for Natural Waters Determined by Molecular Dynamics Simulation. Environ Sci Technol. 2009; 43(9):3183–3186. [PubMed: 19534132]
59. Boehm, HP.; Clauss, A.; Fischer, G.; Hofmann, U. Surface Properties of Extremely Thin Graphite Lamellae; Proceedings of the Fifth Conference on Carbon; 1962. p. 73-80.
60. Buneman O. Computer-Simulation Using Particles - Hockney, Rw, Eastwood, Jw. Siam Rev. 1983; 25(3):425–426.
61. Topsakal M, Sahin H, Ciraci S. Graphene coatings: An efficient protection from oxidation. Phys Rev B. 2012; 85(15)
62. Kirkland NT, Schiller T, Medhekar N, Birbilis N. Exploring graphene as a corrosion protection barrier. Corros Sci. 2012; 56:1–4.
63. Kim BH, Kim JY, Jeong SJ, Hwang JO, Lee DH, Shin DO, Choi SY, Kim SO. Surface Energy Modification by Spin-Cast, Large-Area Graphene Film for Block Copolymer Lithography. ACS Nano. 2010; 4(9):5464–5470. [PubMed: 20738125]
64. Hwang JO, Lee DH, Kim JY, Han TH, Kim BH, Park M, No K, Kim SO. Vertical ZnO nanowires/graphene hybrids for transparent and flexible field emission. J Mater Chem. 2011; 21(10):3432–3437.

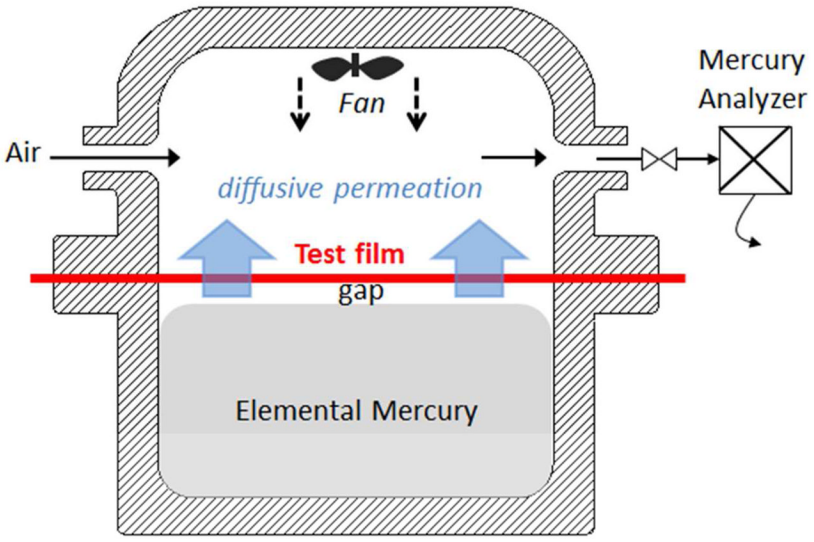

Figure 1.
Custom glass diffusion cell developed for measurement of Hg-vapor permeability through polymer and polymer/graphene sheet materials. A narrow gap (2mm) below the film and forced convection above are features needed to minimize gas-phase mass transport barriers and isolate the test film resistance.

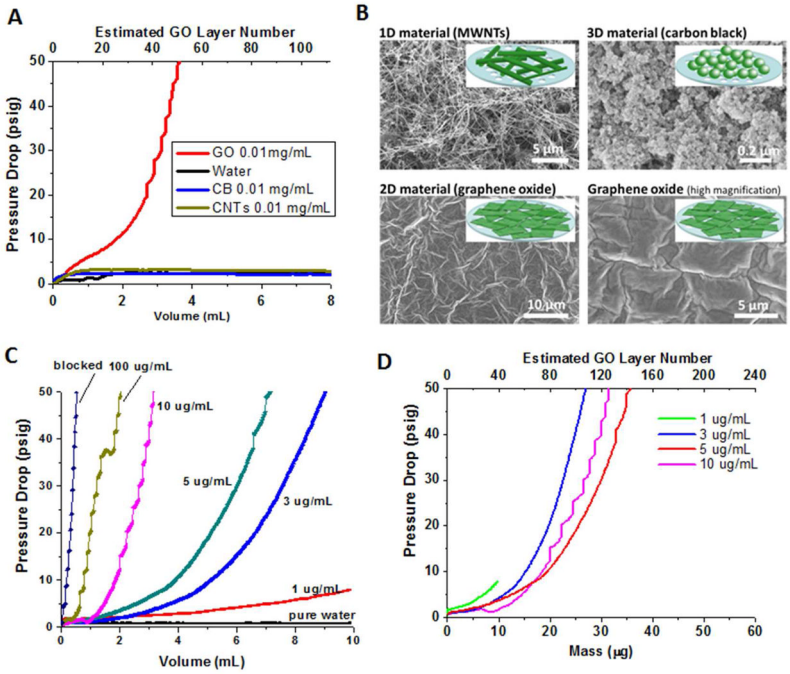

Figure 2.

Demonstration of graphene oxide as a hydraulic sealant. A. Pressure drop during forced filtration through nanochannel alumina filters (20 nm pore size) for graphene oxide compared to carbon black material) and carbon nanotubes (2D material), which form three-dimensional porous filter cakes; B. SEMs showing structure of deposited films or porous filter cakes; C. Concentration dependence of sealant effect for GO and Nylon filters. Label "blocking" refers to a control experiment in which the syringe was capped; D. Unification of panel C. data by renormalizing X-axis as the total mass of GO deposited ($M = C \cdot V_{filtration}$)

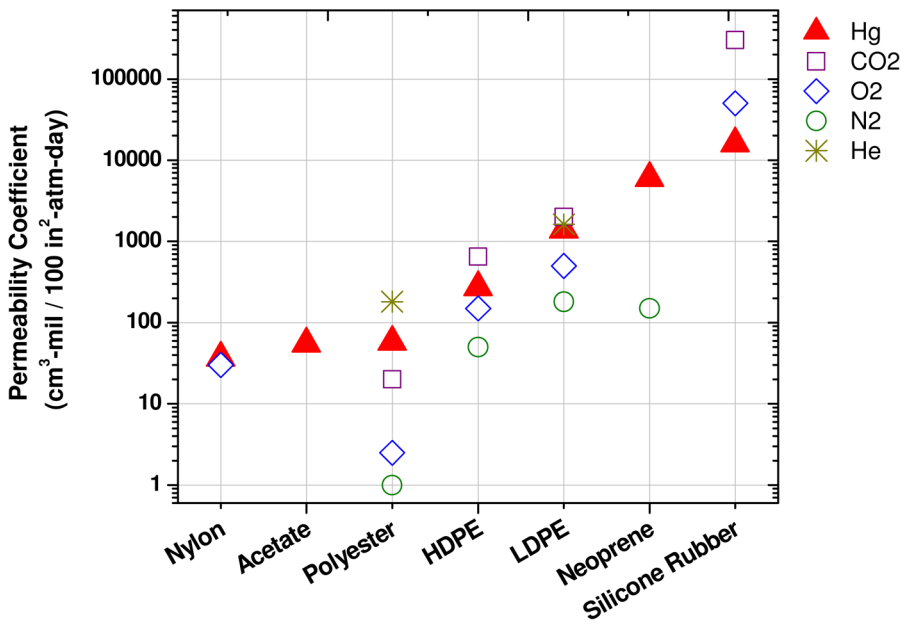

Figure 3.

Measured Hg-vapor permeability coefficients (solid markers) for common commercial polymer sheet materials. Literature values for small gases in the same materials included for comparison [25]

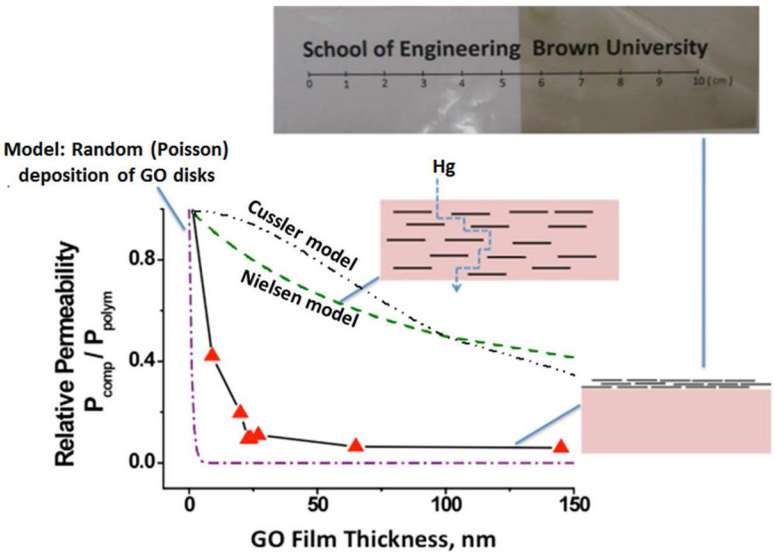

Figure 4.

Effectiveness of thin graphene oxide films as Hg-vapor barrier enhancers on 50 μm polyester. The film configuration is seen to be much more effective than the common configuration with GO uniformly mixed (compounded) with the polymer (Nielsen model; Cussler model[26–29]). The data lie between the Nielsen ideal imbedding limit and the limit for random overlapping disks whose centers of mass deposit on the film by a Poisson process. For the modeling, the atomic GO thickness was taken as 1 nm and the lateral dimension 1 μm. Image shows polyester film treated with GO film (right) and untreated (left).

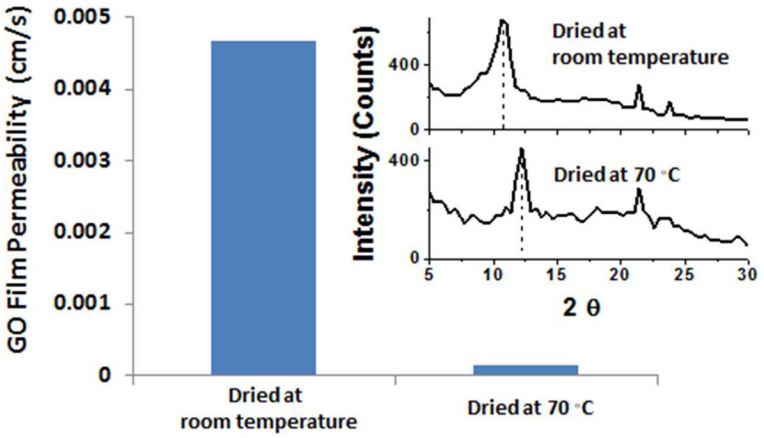

Figure 5.

Effect of drying conditions on the interlayer spacing and Hg permeability of GO films. The permeability of films dried at room temperature at 15 % relative humidity for 48 hours (left), and at approximately 70°C with zero relative humidity for 48 hours (right). The inserted X-ray diffraction (XRD) spectra show that these two drying conditions lead to interlayer spacings of 0.82 nm and 0.73 nm respectively. These GO films have an areal density of 35 mg/m^2 and approximately 25 layers.

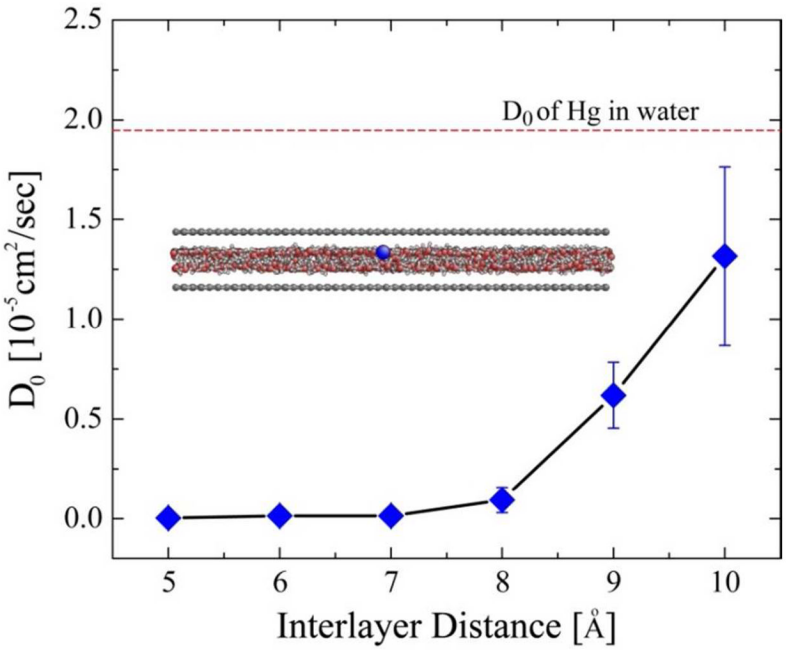

Figure 6.

Molecular dynamics (MD) simulations of Hg-atom diffusion in graphene interlayer spaces containing water. The diffusivity of a tracer Hg-atom is seen to decrease with decreasing interlayer spacing, and Hg becomes immobile below 7 Å spacing. Inset shows a graphene interlayer region with with 8 Å spacing, and one mercury atom (blue) in water (red-grey beads). The dashed line gives the known diffusivity of Hg in bulk water.

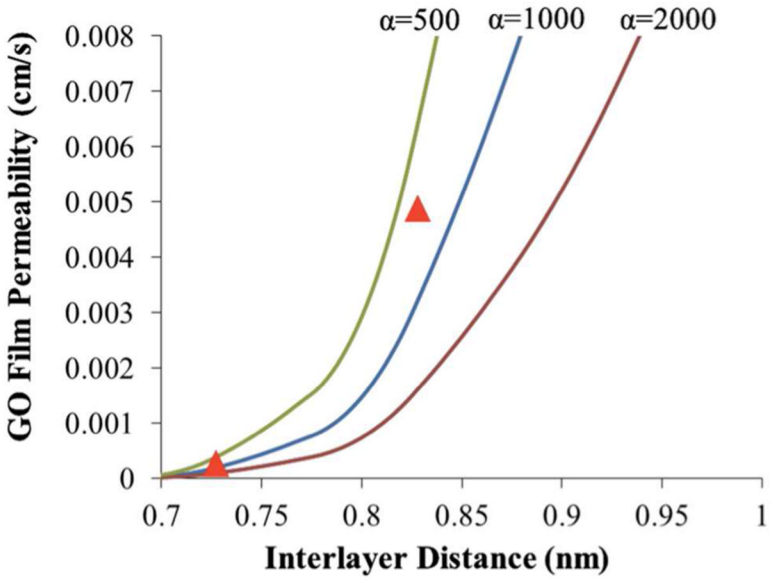

Figure 7.

Results from the Nielsen model modified for excluded volume and using the Hg diffusivity values obtained by MD simulation in Fig. 6. The curves are predictions for 25 nm GO films with various values of GO aspect ratio, α. The triangles give the measured results from Fig. 5. These results support the hypothesis that the higher Hg permeability in wet films is due to the increase in interlayer spacing associated with water pillaring, which allows lateral diffusion of Hg atoms through the expanded and hydrated interlayer spaces. More complete drying reduces interlayer spacing and restricts lateral Hg diffusion, which leads to lower permeability.